Author/s:
Saini, H;Pontes, G;Brown, JR;Drysdale, RN;Du, Y;Menviel, L

Title:
Australasian Hydroclimate Response to the Collapse of the Atlantic Meridional Overturning Circulation Under Pre-Industrial and Last Interglacial Climates

Date:
2025-03-01

Citation:
Saini, H., Pontes, G., Brown, J. R., Drysdale, R. N., Du, Y. & Menviel, L. (2025). Australasian Hydroclimate Response to the Collapse of the Atlantic Meridional Overturning Circulation Under Pre-Industrial and Last Interglacial Climates. Paleoceanography and Paleoclimatology, 40 (3), https://doi.org/10.1029/2024PA004967.

Persistent Link:
https://hdl.handle.net/11343/369440

Paleoceanography and Paleoclimatology

AGU ADVANCING EARTH AND SPACE SCIENCES

RESEARCH ARTICLE
10.1029/2024PA004967

Key Points:

- An Atlantic Meridional Overturning Circulation (AMOC) collapse leads to wetter conditions over northern Australia during austral summer
- The Maritime Continent between 5°S and 6°N, southern Australian region, and New Zealand, display drier conditions throughout the year
- The difference in background climate states leads to regional differences in the Australian hydroclimate response to an AMOC collapse

Supporting Information:

Supporting Information may be found in the online version of this article.

Correspondence to:

H. Saini,
himadri.saini@unsw.edu.au

Citation:

Saini, H., Pontes, G., Brown, J. R., Drysdale, R. N., Du, Y., & Menviel, L. (2025). Australasian hydroclimate response to the collapse of the atlantic meridional overturning circulation under pre-industrial and last interglacial climates. *Paleoceanography and Paleoclimatology*, *40*, e2024PA004967. https://doi.org/10.1029/2024PA004967

Received 1 JUL 2024
Accepted 8 JAN 2025

Australasian Hydroclimate Response to the Collapse of the Atlantic Meridional Overturning Circulation Under Pre-Industrial and Last Interglacial Climates

Himadri Saini[1,2], Gabriel Pontes[1,2], Josephine R. Brown[3], Russell N. Drysdale[3], Yanxuan Du[3], and Laurie Menviel[1,2]

[1]Climate Change Research Centre, University of New South Wales, Sydney, NSW, Australia, [2]The Australian Centre for Excellence in Antarctic Science, University of Tasmania, Hobart, TAS, Australia, [3]School of Geography, Earth and Atmospheric Sciences, University of Melbourne, Melbourne, VIC, Australia

Abstract Abrupt climate change events during the last glacial period and the Last Interglacial (LIG) resulted from changes in the Atlantic Meridional Overturning Circulation (AMOC). Over the last 50 years, there is some evidence that the AMOC has weakened, and it is projected to weaken further or even collapse this century driven by the increase in atmospheric greenhouse gases. However, the impact of an AMOC weakening on Australasian hydroclimate is still unclear, particularly under a climate warmer than the pre-industrial (PI). Using the ACCESS-ESM1.5 model, we assess the processes impacting seasonal hydroclimate in the Australasian region in response to an AMOC shutdown under PI and the LIG climatic conditions. While the broad hydroclimate response to an AMOC shutdown is similar in both experiments, notable regional differences emerge, highlighting the influence of background climate states. During austral summer (DJF), the AMOC shutdown leads to drier conditions over the Maritime Continent between 5°S and 6°N and increased precipitation over northern Australia under both PI and LIG conditions. However, the precipitation increase over Australia is weaker under PI than LIG. During austral winter (JJA), mid to high southern regions of Australia and New Zealand experience drying in response to the AMOC shutdown under PI boundary conditions, while under LIG boundary conditions, only southeastern Australia and New Zealand exhibit drier conditions, with northwestern Australia displaying wetter conditions. These results underscore the complex and region-specific responses of Australasian hydroclimate to AMOC disruptions, highlighting the importance of considering background climate states when assessing such impacts.

1. Introduction

The Atlantic Meridional Overturning Circulation (AMOC) is a critically important system of ocean currents that redistributes heat in the Atlantic Ocean. The AMOC transport has been weakening over recent decades (Caesar et al., 2018; Thornalley et al., 2018), decreasing by ∼15% since the middle of the twentieth century (Caesar et al., 2018; Jackson et al., 2022; Latif et al., 2022; Rahmstorf et al., 2015; Smeed et al., 2018), and there is a growing consensus that it is at its weakest of the last millennium (Caesar et al., 2021). The fifth and sixth phases of the Coupled Model Intercomparison Project (CMIP5 and CMIP6) future scenarios suggest that the AMOC might weaken by 34%–45% (between 6 and 8 Sv) by the end of the current century under the ssp5-8.5 scenario (Weijer et al., 2020). Furthermore, studies based on early warning signals suggest that the AMOC could collapse before the end of the century (Boers, 2021; Ditlevsen & Ditlevsen, 2023).

Paleoclimate records and modeling studies have indicated that the AMOC weakened significantly on a multi-centennial timescale during the Quaternary, and particularly during Heinrich stadials (HS) (Lynch-Stieglitz, 2017; Menviel et al., 2020; Rahmstorf, 2002). While most of the periods of AMOC weakening occurred during glacial periods or deglaciations, there is evidence for AMOC weakenings during the Last Interglacial period (LIG, 129,000 to 116,000 years ago (ka)) (Galaasen et al., 2014; Tzedakis et al., 2018), as well as previous interglacials (Galaasen et al., 2020). Significant AMOC weakening is thus not exclusive to glacial climates and it is important to understand the climatic impacts of such a weakening under interglacial climates, such as the LIG.

Several modeling studies have investigated the impact of an AMOC weakening or shutdown on global climate. Since most of the AMOC weakening events occurred during glacial periods (Henry et al., 2016), many modeling studies of AMOC weakening have been performed under glacial conditions (Kageyama et al., 2013; Menviel, England, et al., 2014; Menviel et al., 2008; Saini et al., 2024), but some have also been performed under pre-industrial (PI) (Orihuela-Pinto et al., 2022; Stouffer et al., 2006) or present-day conditions (Jackson et al., 2015). In both cases, an AMOC shutdown leads to a weaker northward oceanic heat transport in the Atlantic, inducing a cooling of the North Atlantic and Greenland, as well as warmer conditions over the Southern Ocean and Antarctica. This is in agreement with paleo proxy records from the North Atlantic and Greenland (Buizert et al., 2014; Henry et al., 2016; Huber et al., 2006; Kindler et al., 2014; Menviel et al., 2020), as well as from the Southern Ocean and Antarctica (Blunier & Brook, 2001; Buizert et al., 2015; Jouzel et al., 2007; Pedro et al., 2018; Seidov & Maslin, 2001; Stocker, 1998; Stocker & Johnsen, 2003; Timmermann et al., 2010).

Due to the changes in meridional temperature gradients, an AMOC shutdown results in a southward shift of the Inter-tropical convergence zone (ITCZ) in the Atlantic (Jackson et al., 2015; Menviel et al., 2008; Menviel, England, et al., 2014; Orihuela-Pinto et al., 2022; Vellinga & Wood, 2002). Multiple proxy records from the Atlanticsector support a southward shift of the ITCZ during HS, manifested as a decrease in precipitation in parts of northern Venezuela (Deplazes et al., 2013; Haug et al., 2001; Peterson et al., 2000), northern tropical Africa (McGee et al., 2013; Weldeab et al., 2007), and central America (Escobar et al., 2012) and an increase in precipitation in the southern tropical regions of Brazil, Africa and some other parts of South America (Gasse, 2000; Jennerjahn et al., 2004; X. Wang et al., 2004; Cruz et al., 2009; Ciemer et al., 2021).

By contrast, the impact of an AMOC shutdown on the Australasian climate remains uncertain, as no modeling study has thoroughly examined the processes affecting Australasian precipitation in the aftermath of such an event. Furthermore, paleo-records show inconsistent signals, likely influenced by a range of factors present at the time, including different orbital parameters, vegetation cover, and other environmental conditions. The longest speleothem record, spanning the last 55.7 ka, suggests inconsistencies in the strength of the Indonesian-Australian summer monsoon (IASM) during different HS, involving an AMOC shutdown (Scroxton et al., 2022). For instance, some records indicate a precipitation decrease in northern Australia during Heinrich stadial 3 (HS3, 30.1 to 27.8 ka) despite a southward migration of the ITCZ (Lewis et al., 2011; Scroxton et al., 2022). In contrast, several terrestrial paleo records from northern Australia (Denniston et al., 2013; Muller et al., 2008) indicate increased precipitation or a stronger IASM, whereas records from northern Borneo (Partin et al., 2007) and southern Java (Mohtadi et al., 2011) indicate reduced precipitation during Heinrich stadial 1 (HS1, 17.6 to 14.6 ka). On the other hand, Muller et al. (2012), Ayliffe et al. (2013), and Scroxton et al. (2022) suggest increased precipitation in the Flores Sea during HS1. In addition, HS1 could have been influenced by additional deglacial processes, such as rising sea levels, increasing greenhouse gas concentrations, and ice-sheet retreat, further complicating its interpretation. The ambiguity in these records could also be attributed to the lack of high resolution and temporal continuity, as well as uncertainty in estimating the total precipitation amounts from different proxy types. Additionally, due to the complex geographic setting, obtaining proxy records at all necessary locations is impractical. Therefore, climate modeling provides a viable path forward, which can also help explain apparent anomalies between proxy records. Finally, no records with sufficient resolution to resolve AMOC variability are available for mid-latitude or southern Australia, regions, which are impacted by processes beyond the ITCZ.

To address this uncertainty regarding the Australasian climate's response to an AMOC shutdown, particularly under warmer climates, our study examines the hydroclimate changes across the Australasian region in response to an AMOC weakening under both PI and LIG conditions. The LIG not only exhibits evidence of AMOC weakening (Galaasen et al., 2014; Tzedakis et al., 2018) but also stands out as the warmest interglacial of the last 800 ka (Masson-Delmotte et al., 2013). From now on, the LIG refers to the climatic optimum, which occurred at ~127 ka. The LIG was characterized by a minimum precession index, whereas the PI has a relatively high value (Berger, 1978). This lower precession, combined with greater obliquity and eccentricity than PI, led to higher boreal summer insolation during the LIG (Laskar et al., 2004), potentially causing a northward shift of the ITCZ compared to PI (Yeung et al., 2021). Global mean sea-surface temperatures (SST) during the LIG were 0.2 to 0.8°C higher than PI (Hoffman et al., 2017), with summer air temperatures over northern high latitudes 4 to 5°C higher (Clark & Huybers, 2009), and global sea levels ~2–5 m higher than PI (Dutton & Lambeck, 2012; Dyer et al., 2021; Kopp et al., 2009). In addition, the LIG was preceded by HS11 (~135−128 ka (Tzedakis et al., 2018)), during which the AMOC might have weakened significantly (Menviel et al., 2019). Given the dating uncertainties associated with early LIG proxy records, the Paleoclimate Model Intercomparison Project 4 (PMIP4) LIG protocol also includes a LIG simulation with an AMOC shutdown (Otto-Bliesner et al., 2017) to provide information on the climate state during the later part of HS11.

Here, we perform North Atlantic water hosing experiments using an Earth System Model to investigate the Australasian precipitation response to an AMOC shutdown under both LIG and PI boundary conditions. This allows us to assess the impact of the background climate state on an AMOC shutdown. Furthermore, evaluating the impact of an AMOC collapse under warm climates is particularly relevant in the context of current and projected AMOC weakening.

2. Methods

2.1. Model

In this study, we use the Australian Community Climate and Earth System Simulator-Earth System Model version 1.5 (ACCESS-ESM1.5, Ziehn et al. (2020)). The atmospheric model component is the UK Met Office Unified Model version 7.3 (Martin et al., 2010; The HadGEM2 Development Team: Martin et al., 2011) at N96 resolution (1.875 °× 1.25° and 38 vertical levels). It is coupled to the land surface model, the Community Atmosphere Biosphere Land Exchange model (CABLE) version 2.4 (Kowalczyk et al., 2013), which incorporates biogeochemistry utilizing the CASA-CNP module (Y. Wang et al., 2010). The ocean component is the NOAA/GFDL Modular Ocean Model version 5 (Griffies, 2012), which has a resolution of 1°× 1° (increasing to 0.4° in the Southern Ocean and 0.33° near the equator) with 50 vertical levels. MOM5 is coupled to the Los Alamos National Laboratory sea-ice model version 4.1 (Hunke et al., 2010). Additionally, the coupler utilized in this model for the ocean, sea-ice and atmosphere interaction is the Ocean Atmosphere Sea Ice Soil—Model Coupling Toolkit (Craig et al., 2017). Lastly, the ocean carbon cycle is simulated based on the nutrient, phytoplankton, zooplankton and detritus scheme in the Whole Ocean Model of Biogeochemistry And Trophic-dynamics model (Oke et al., 2013). This model has been evaluated for historical climate and performs well in simulating the climate of the Australasian region (Ziehn et al., 2020).

2.2. Experimental Design

2.2.1. Control Simulations

We use the equilibrium simulations of the PI (*piControl*, Eyring et al. (2016)), and the LIG (*lig127k*, Yeung et al. (2021)) periods, performed with the ACCESS-ESM1.5, to conduct freshwater perturbation experiments. *piControl* is forced with orbital parameters corresponding to 1850 CE and an atmospheric CO_2 concentration of 284.3 ppm. *lig127k* is initialized from *piControl* and is forced by LIG boundary conditions representative of 127 ka (orbital parameters and greenhouse gases, Yeung et al. (2021)) following the PMIP4 protocol (Otto-Bliesner et al., 2017). As such, the LIG atmospheric CO_2 level is set at 275 ppm. The vegetation and ice sheet cover in the *lig127k* simulation are kept constant at PI values and both experiments use a solar irradiance of 1365.65 Wm^{-2}. The total integration length for *piControl* is 1,100 years and 925 years for *lig127k*. We analyze the last 100 years of each simulation. A comprehensive description of *piControl* and *lig127k* control simulations is provided in Ziehn et al. (2020) and Yeung et al. (2021).

2.2.2. Freshwater Perturbation Experiments

To explore the impact of an AMOC collapse on Australian hydroclimate, we artificially add freshwater in the subpolar North Atlantic (SPNA; 50°N-70°N and 70°W-0°E) to mimic Greenland ice sheet runoff as well as iceberg discharge. The SPNA is found to be the main region of iceberg melting as indicated by the presence of ice-rafted debris in marine sediment cores that span the last glacial cycle (Muschitiello et al. (2019) + references within).

We apply a constant 0.4 Sv freshwater flux in the SPNA to simulate a gradual AMOC collapse in the ACCESS-ESM1.5 model. The freshwater perturbation experiments, PIfw and LIGfw were started at year 1,000 from *piControl* and year 850 from *lig127k*, respectively, and were run for 200 years each. A collapsed AMOC state (defined here as an AMOC weaker than 5 Sv) is reached within approximately 150 years in both scenarios (Figure S1 in Supporting Information S1). AMOC strength is calculated as the maximum value of the overturning streamfunction between 30°N and 50°N.

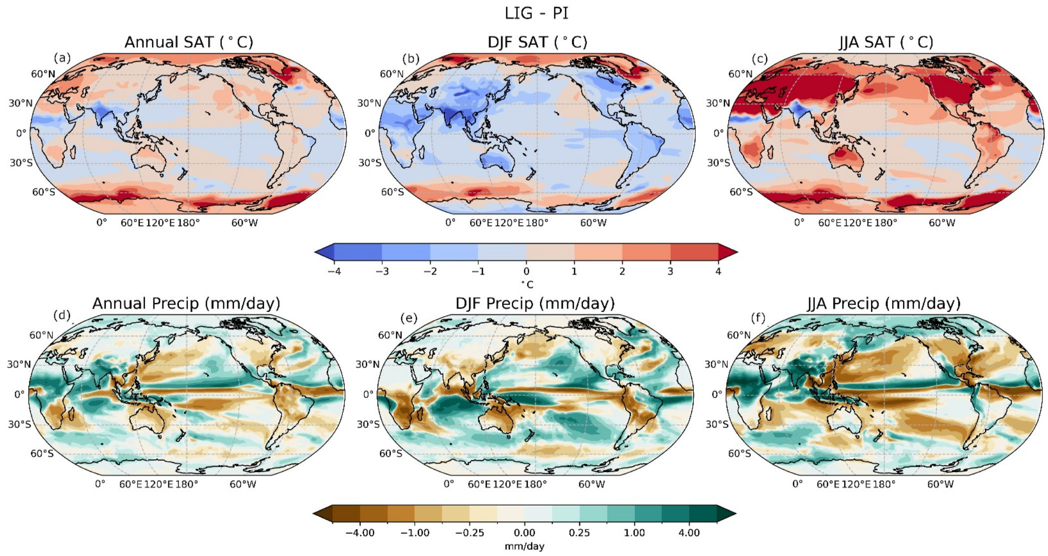

Figure 1. (a), (d) Annual, (b), (e) DJF, and (c), (f) JJA anomalies of (top) surface air temperature (°C) and (bottom) precipitation (mm/day) at the Last Interglacial (*lig127k*) compared to pre-industrial (*piControl*).

2.3. Analytical Approach

Here we analyze the 50 years average from years 150–200 of both perturbation runs. We refer to the anomalies between LIGfw and *lig127k* as LIGfw-lig127k and between PIfw and *piControl* as PIfw-piControl. We focus our analysis on LIGfw-lig127k and summarize the main differences between LIGfw-lig127k and PIfw-piControl briefly. As the Australasian precipitation is governed by different processes in austral summer (December, January, February or DJF) and winter (June, July, August or JJA), our analysis focuses on DJF and JJA.

Monsoon regions are characterized as areas where the rainfall during the monsoon period exceeds that of the dry season by a minimum of 2.5 mm d^{-1}, and where this rainfall accounts for no less than 55% of the total annual precipitation (B. Wang et al., 2011). The total precipitated water is calculated as the product of the monsoon domain's areal extent and the mean precipitation rate within this domain.

The ITCZ position is calculated using the precipitation centroid index (Braconnot et al., 2007). In this index, the ITCZ position is defined as the latitude that divides the tropics (20°S and 20°N) into two region of equal precipitation, which is physically equivalent to the center of gravity of tropical precipitation.

The northern (southern) Hadley cell strength is calculated as the maximum (minimum) value of the atmospheric mass streamfunction between 400 and 600 hPa. Meanwhile, the meridional oceanic heat transport is calculated from the meridional temperature advection flux at 30°N.

3. Results

3.1. Brief Overview of the LIG (127 ka) Climate as Simulated by the ACCESS-ESM1.5

Overall, the simulated global mean annual surface air temperature (SAT) and SST are 0.4°C and 0.2°C higher during LIG compared to PI, respectively. Due to strong boreal summer (JJA) insolation anomalies (e.g., +70 Wm^{-2} in June at 80°N) at 127 ka, driven by low precession and greater obliquity and eccentricity, the JJA mean SAT at 40°N−60°N is 6.5°C higher at the LIG than PI (Figure 1). Conversely, in the Southern Hemisphere (SH) at 40–60°S, JJA SATs are only 0.4°C higher during the LIG than PI. During DJF, LIG SATs are 1°C lower in the Northern Hemisphere (NH) due to negative insolation anomalies (reaching approximately −45 Wm^{-2} at 40°S), with enhanced cooling over land between 40°N and 40°S. SATs are 1°C higher in the Southern Ocean due to lower sea-ice extent compared to PI (Figure 1, Yeung et al. (2024)). Due to the inter-hemispheric temperature contrast, the global ITCZ is shifted 1° northward in JJA at the LIG (situated at 6.7°N) compared to PI (situated at 5.6°N), while it is shifted southward in DJF over the oceans, even though the response in the Pacific sector is more complex (Figure 1 and Figure S2 in Supporting Information S1). Furthermore, weaker insolation anomalies

10.1029/2024PA004967

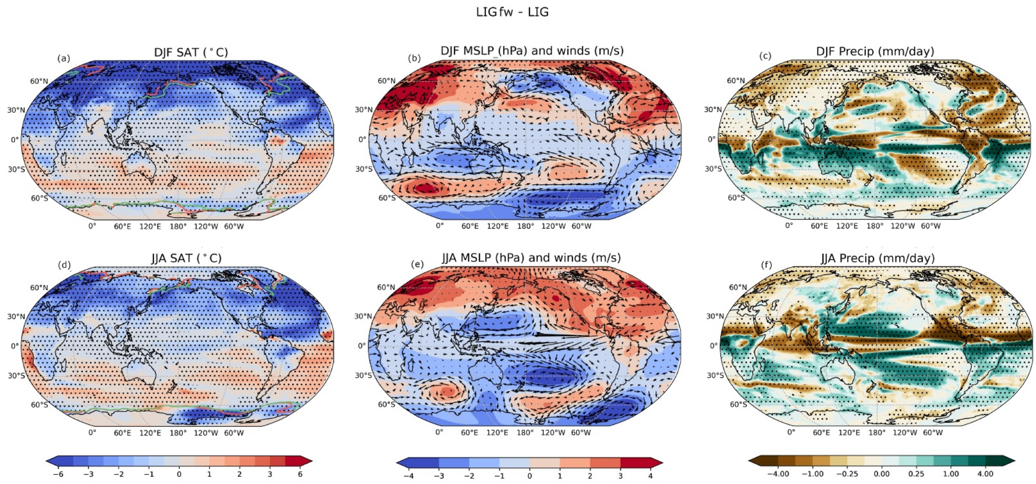

Figure 2. Changes in (a), (d) surface air temperature (°C) (b), (e) mean sea level pressure (hPa) overlaid with surface wind anomaly (m/s) and (c), (f) precipitation (mm/day) as a response to an AMOC shutdown in LIGfw compared to *lig127k* during (top) DJF and (bottom) JJA. Stippling indicates significant changes based on a Student's *t*-test at 95% significance level.

during DJF at the LIG compared to PI lead to significantly larger cooling over land regions than over the ocean in most of the SH. This causes an increase in sea-level pressure and thus subsidence over land, resulting in a weaker Australian monsoon during the LIG compared to PI (Yeung et al., 2021). The detailed description of the simulated LIG climate, differences between the *lig127k* and *piControl* simulations, its characteristics compared to other *lig127k* PMIP4 simulations, and comparison with proxy records have been described in detail in previous studies (Kageyama et al., 2020; Otto-Bliesner et al., 2021; Yeung et al., 2021, 2024).

3.2. Large Scale Climate Response to an AMOC Shutdown

In the LIGfw simulation, the shutdown of the AMOC results in a 66% reduction in northward oceanic heat transport at 30°N in the Atlantic. This leads to a SST decrease and a DJF sea-ice advance of 30° eastward in the Labrador Sea and 6° southward in the Nordic Seas, which induces a 7.5°C decrease in winter SATs over the North Atlantic (Figure 2a). Similarly, in the Northwest Pacific, temperature decreases by 5°C and sea-ice advances 9° eastward, linked to a deepening of the Aleutian low. Meanwhile, the reduced northward oceanic heat transport, causes a slight warming of 0.6°C in the South Atlantic (0°S−40°S) during DJF, extending to the north of the Antarctic Circumpolar Current and into the south Indian and Pacific Oceans. Minimal sea-ice changes are simulated in the Atlantic and Indian Ocean sectors of the Southern Ocean, while a 7° northward shift of the sea-ice edge is simulated in the Pacific. In JJA, the North Atlantic cools, pushing the sea-ice edge 11° further east in the Labrador Sea and 6° further south in the Nordic Seas (Figure 2d green line), and leading to a 5.6°C SAT decrease in LIGfw-lig127k (Figure 2d). The North Pacific also experiences a cooling of about 3°C. In contrast, a 0.7°C warming is simulated in the South Atlantic in LIGfw-lig127k, with a smaller warming of 0.03° in the Indo-Pacific region between 0°S−40°S. No significant sea-ice changes are simulated over the Indian sector, while a 5° increase in sea-ice extent in the Bellinghausen Sea and an 8° eastward extension in the Weddell Sea are associated with cooling south of 60°S.

The overall cooling in the NH strengthens the subtropical semi-permanent high-pressure system over the North Atlantic Ocean, with a smaller intensification over Asia during both DJF and JJA (Figures 2b and 2e and Figures S3b and 3e in Supporting Information S1). The large-scale spatial climate response to the simulated AMOC shutdown under PI (PIfw) and LIG (LIGfw) boundary conditions is broadly similar but the amplitude of the changes differs (Figure 2 and Figure S3 in Supporting Information S1). Further details on these differences are discussed in Section 4.1.

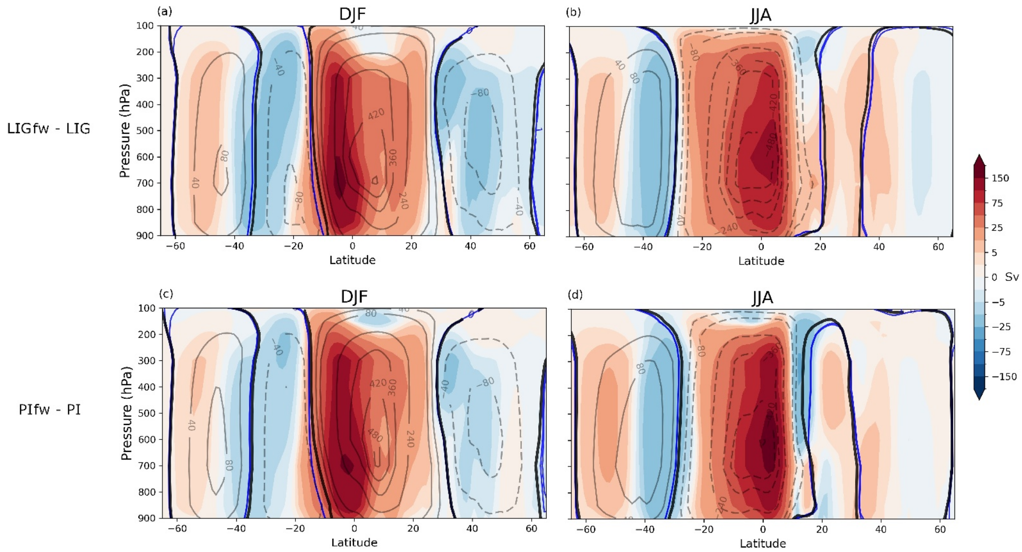

Figure 3. Atmospheric mass streamfunction (Sv) anomalies (shading) for (top) LIGfw minus *lig127k* and (bottom) PIfw minus *piControl* averaged over (a), (c) DJF, and (b), (d) JJA. Contours (solid is positive; dashed is negative) indicate *piControl* and *lig127k* control mean. The thick black and blue lines represent the zero contour in the control experiments and the FW experiments, respectively.

3.3. Precipitation Response to an AMOC Shutdown Over Australasia

3.3.1. Austral Summer (DJF) Precipitation Changes

To compensate for the 40% reduction in global northward oceanic heat transport at 30°N, the NH Hadley cell strengthens by ∼14% and shifts 2° southward in LIGfw during DJF (from 8.2°S to 10°S, Figure 3a). This stronger and shifted Hadley cell causes a 2° southward displacement of the global ITCZ (Figure 2c and Figure S2a in Supporting Information S1). As the ITCZ shifts south, the LIGfw displays drier conditions over the Maritime Continent between 5°S and 6°N, including Sumatra, Borneo, Indonesia and northern part of Papua New Guinea, along with increased austral summer precipitation over northern Australia compared to *lig127k* (Figure 4a). This increase is attributed to the cyclonic circulation associated with the low-pressure anomaly over the Indian Ocean

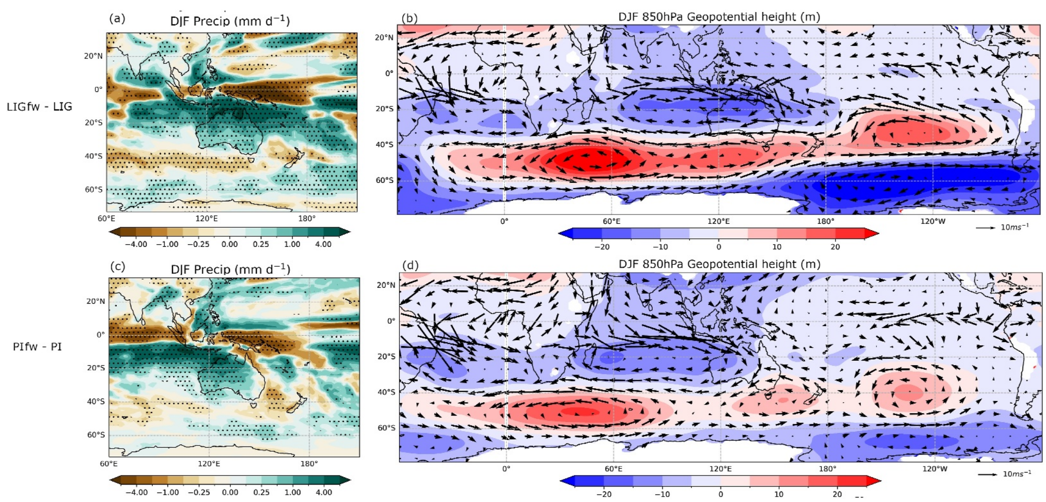

Figure 4. Changes in (a), (c) precipitation (mm/day) and (b), (d) geopotential height (m) at 850 hPa overlaid with wind anomaly (m/s) at 850 hPa as a response to an Atlantic Meridional Overturning Circulation shutdown for (top) LIGfw compared to *lig127k* and (bottom) PIfw compared to *piControl* during austral summer (DJF). Stippling indicates significant changes based on a Student's *t*-test at 95% significance level.

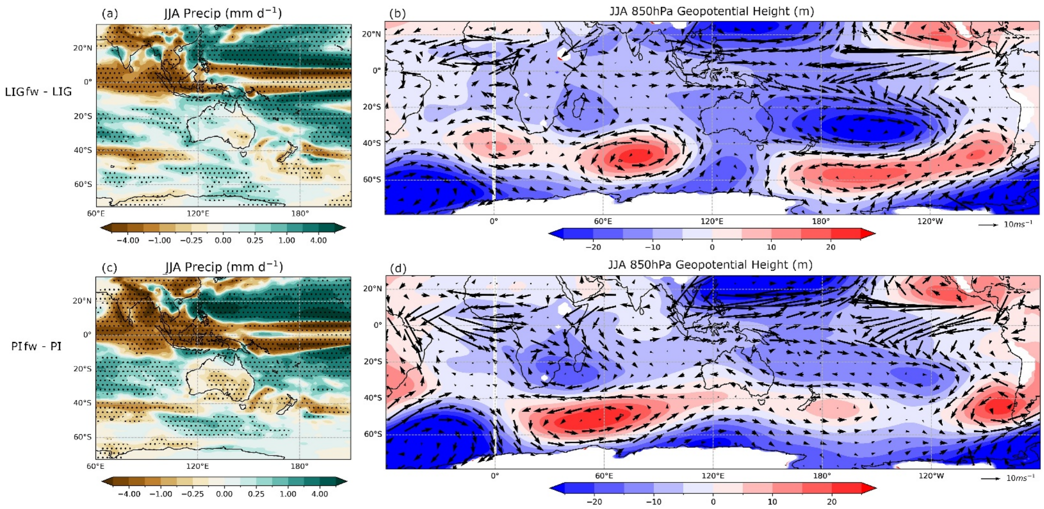

Figure 5. Changes in (a), (c) precipitation (mm/day) and (b), (d) geopotential height (m) at 850 hPa overlaid with wind anomaly (m/s) at 850 hPa as a response to AMOC shutdown for (top) LIGfw compared to *lig127k* and (bottom) PIfw compared to *piControl* during austral winter (JJA). Stippling indicates significant changes based on a Student's *t*-test at 95% significance level.

(Figure 4b), which stems from a Rossby wave train that originates from the equatorial Atlantic, triggered by stronger tropical convection due to increased SSTs in that region. Consequently, the areal extent of the Australian monsoon domain expands by 73% in the LIGfw experiment in comparison to *lig127k*, accompanied by a 81% rise in total precipitated water within this domain during the monsoon season (Figure S4 in Supporting Information S1).

The drying pattern simulated south of Australia, including Tasmania and New Zealand, results from the changes in the SH subtropical high-pressure systems, typically located between 20°S and 40°S in the Indian, Pacific, and Atlantic oceans in *piControl* (Figure S5 in Supporting Information S1). In LIGfw, these high-pressure systems shift southward due to the (1.5°) southward displacement of the SH Hadley cell, while the intensification of the Hadley cell (by 12%) leads to a high-pressure anomaly south of 40°S, resulting in drying in this region. Additionally, this displacement of the high-pressure systems further shifts the rain-bearing storm tracks southward leading to drier conditions over Australia (including Tasmania) and New Zealand. A similar, but weaker, pattern of precipitation change and circulation shift is simulated in PIfw-piControl (Figure 4), as discussed in Section 4.1.

3.3.2. Austral Winter (JJA) Precipitation Changes

During JJA, the SH Hadley cell in LIGfw weakens by 20% and shifts slightly southward (≤1°) compared to *lig127k* (Figure 3b). Meanwhile, the global ITCZ shifts south by 1.5° (Figure S2e in Supporting Information S1), with a more pronounced 5° shift extending from the eastern equatorial Pacific to the eastern side of the African continent (Figures 2f and S2h). However, in the western Pacific, no ITCZ shift is simulated, though rainfall within the ITCZ decreases (Figure S2g in Supporting Information S1). Colder conditions are also simulated over the Maritime Continent and central Pacific (Figure 2d). Additionally, while the north-easterlies are stronger in the eastern equatorial Pacific, the easterlies weaken in the western equatorial Pacific (Figure 5b). As a result, there is a 13% decrease in precipitation over the Maritime Continent between 6°S and 10°N (Figure 5a).

The Australian precipitation response during JJA is less significant and more complex than in DJF. The weakening of the SH Hadley cell leads to wetter conditions in the northwestern part of the continent (122°E−135°E, 25°S−15°S). However, drier conditions are simulated in the southeastern sector (142°E−152°E, 34°S−29°S) and New Zealand due to the southward shift of the Ferrell cell (Figure 3b) which intensifies the high-pressure system south of Australia, diverting incoming frontal systems and causing further drying in the region (Figure 5a).

Finally, southern Australia, which experiences its rainy season during JJA due to mid-latitude westerlies bringing precipitation, also becomes drier. The weakening of the westerlies between 30°S and 45°S associated with a southward shift in both the Indian and Pacific sectors of the Southern Ocean (Figure 5b), further contributes to the drier conditions in southeastern Australia and New Zealand in LIGfw-lig127k during JJA. The drier conditions in PIfw-picontrol are more significant and discussed in the next section.

4. Discussion

As Australasian summer and winter rainfall are governed by different processes and feedback, we analyze the seasonal changes separately. During austral summer (DJF), the Australian monsoon dominates, particularly in northern Australia. The ITCZ shifts to its southernmost position, bringing moisture-laden winds from the warm tropical oceans. This results in enhanced convection and increased rainfall over northern Australia and the Maritime Continent (Figure S5c in Supporting Information S1). In winter (JJA), southern Australia and parts of New Zealand experience heightened rainfall due to the strengthening of the mid-latitude westerlies and the passage of cold fronts (Figure S5f in Supporting Information S1). These westerlies are linked to the Southern Ocean storm tracks, which transport moisture from the ocean into southern Australia.

An AMOC shutdown under LIG climate affects the interhemispheric thermal gradient, with a colder NH and a warmer SH. This plays a crucial role in shaping atmospheric circulation patterns, causing the intensification and southward shift of both the northern and southern Hadley cells during DJF. The magnitude of large-scale changes associated with AMOC shutdown under both PI and LIG climates, such as the temperature response in the North and South Atlantic, are consistent with previous modeling simulations performed under PI or glacial boundary conditions (Jackson et al., 2015; Kageyama et al., 2013; Menviel et al., 2008; Menviel, Timmermann, et al., 2014; Saini et al., 2024; Stouffer et al., 2006; Timmermann et al., 2010; Vellinga & Wood, 2002), including the deepening of the Aleutian low (Okumura et al., 2009). The shift in the northern Hadley cell pushes the ITCZ southward, leading to drying over Sumatra, Borneo, Indonesia, and the northern part of Papua New Guinea, while northern Australia experiences wetter conditions during DJF. The simulated 2° southward shift of the global ITCZ is in agreement with the above-mentioned modeling studies as well as some proxy records indicating such a shift during the AMOC weakening episode of HS1 (Denniston et al., 2013; McGee et al., 2014). The warming in the Tropical South Atlantic region results in enhanced atmospheric convection triggering a stationary Rossby wave train that propagates from the equatorial Atlantic toward the Australian continent. This wave train establishes a low-pressure anomaly over Australia, inducing cyclonic circulation with reinforced onshore northwesterly flow. This enhances the moisture transport, contributing to increased precipitation over northern Australia. In the southern Australian and New Zealand sectors, the southward shift of the SH Hadley cell displaces semi-permanent high-pressure systems south of 40°S, creating a high-pressure anomaly in that area and consequently leading to drier conditions. The high-pressure anomaly also blocks incoming cold fronts toward southern Australia, leading to further drying.

During austral winter (JJA), while there is a 5° southward shift of the ITCZ in the equatorial Atlantic, only a weakening of the ITCZ is simulated over the Indian Ocean and in the western Pacific. Drier conditions are thus simulated over the Maritime Continent between 6°S and 10°N. The weakening of the SH Hadley cell leads to anomalous wetter conditions in the northwestern region of Australia, while the drier conditions over the southeastern region result from the southward shift of the Ferrel cell and southward shift in high-pressure systems. However, the overall response over northwestern and southeastern Australia is relatively insignificant.

4.1. Dependence on the Background State

While the climatic impact of an AMOC shutdown is broadly similar under LIG and PI conditions, some regional differences are simulated. A normalization of the climatic changes by the magnitude of the AMOC decrease (Figure S6 in Supporting Information S1) — that is larger in LIGfw-lig127k than in PIfw-piControl (Table S1 in Supporting Information S1) — suggests that outside of the Atlantic basin, the different climatic anomalies in LIGfw-lig127k compared to PIfw-piControl are due to the different initial climate state, resulting from different insolation.

Due to the high boreal summer insolation in JJA at the LIG, the ITCZ is displaced northward in all ocean basins compared to the PI state. In DJF, the ITCZ is also displaced northward in the Pacific basin, while it is displaced southward over the Indian and Atlantic Oceans. Overall, the global annual mean ITCZ is ~0.4° northward at the LIG compared to PI (Figure 6a), due to a change in meridional temperature gradient (Schneider et al., 2014). This shift likely arises from the low precession at the LIG climate, which placed perihelion during boreal summer, amplifying the seasonal insolation contrast and thus affecting the temperature gradient across hemispheres and the

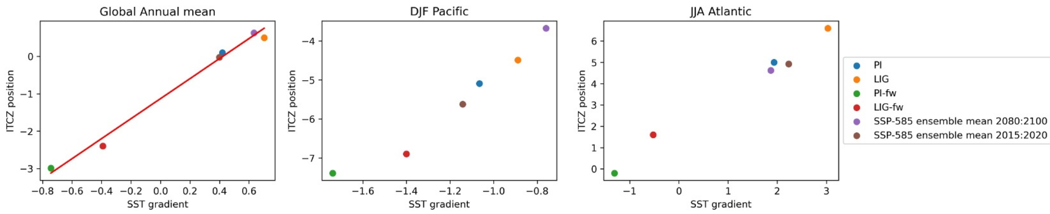

Figure 6. Relationship between the Inter-tropical convergence zone (ITCZ) and the tropical meridional SST gradient (5°N–30°N minus 5°N–30°S) for (blue) pre-industrial (orange) Last Interglacial (green) PIfw and (red) LIGfw simulations: (a) globally averaged annual mean, (b) over the Pacific during DJF, and (c) over the Atlantic during JJA. Results from a 4-member ensemble of CMIP6 SSP5-8.5 simulations performed with the ACCESS-ESM1.5 model are also included to provide context on projected ITCZ shifts under future high-emission scenarios. The inclusion of SSP5-8.5 allows for a comparison between past and future climates, highlighting potential changes in ITCZ dynamics due to anthropogenic warming. Slope in (a) = 2.7°C and r^2 = 0.99.

ITCZ seasonality. However, we do not isolate the specific impacts of precession from the total insolation change here. Future studies that isolate the influence of specific insolation parameters, such as precession or obliquity, could further clarify their role in modulating hydroclimatic responses across the hemispheres, which at the moment remains uncertain (Beaufort et al., 2010; Wyrwoll et al., 2007; Zhang et al., 2022).

In response to the AMOC shutdown, during DJF, PIfw-picontrol displays drying over the Maritime Continent between 5°S and 6°N similar to LIGfw-lig127k (Figures 4a and 4c). The southward ITCZ shift in the Pacific is slightly larger in LIGfw-lig127k than in PIfw-picontrol (Figure 6b) due to the larger meridional temperature contrast (Table S1 in Supporting Information S1). This leads to a stronger intensification of the northern Hadley cell (7%) in LIGfw-lig127k. In addition, the simulated drying south of Australia in DJF is larger in LIGfw-lig127k than in PIfw-picontrol due to the larger positive geopotential height anomaly. These results suggest that the different background state impacts the climatic response in that region.

The absolute temperature increase in the Tropical South Atlantic is slightly larger (by 0.2°C) in LIGfw-lig127k compared to PIfw-piControl due to the larger AMOC decrease in the former (Figure 2, Figures S2 and S6 in Supporting Information S1), which triggers a stronger Rossby wave train toward Australasia. However, it is unlikely that the simulated geopotential differences in the southern Indo-Pacific sector are only due to this small temperature difference. While in LIGfw-lig127k a negative geopotential anomaly is simulated at 850 hPa across Australia in DJF, in PIfw-piControl, the negative anomaly only extends from the Indian Ocean to the north-western part of Australia (Figures 4b and 4d). The reduced extent of the low-pressure anomaly over Australia results in a smaller expansion (by 24%) of the monsoon domain in PIfw-piControl, with the precipitation increase limited to the western and northwestern regions (Figure 4c, Figures S4 and S7 in Supporting Information S1).

During JJA, drying over the equatorial Maritime Continent between 6°S and 10°N is more substantial in PIfw-picontrol than in LIGfw-lig127k (Figure 5). As low precession in the LIG causes a warmer NH during boreal summer, the weakening of the ascending branch of the SH Hadley cell is larger (by 5%) for an AMOC collapse under PI than under LIG conditions (Table S1 in Supporting Information S1, Figures 3b and 3d). Thus, leading to a stronger drying over the Maritime Continent in PIfw. Additionally, the descending branch of the SH Hadley cell in PIfw exhibits a larger 2° southward shift and strengthening compared to LIGfw (Figure 3d). This leads to significantly drier conditions across Australia during JJA in PIfw (Figure 5c), in contrast to the relatively muted response in LIGfw.

In the Atlantic basin, the southward ITCZ shift during JJA in LIGfw-lig127k and PIfw-piControl has a similar amplitude and scale with the change in meridional SST gradient (Figure 6c). Despite LIGfw and PIfw having a similar AMOC strength, the ITCZ is still shifted northward in LIGfw compared to PIfw due to the different insolation forcing. Figure 6 indicates that while there is a linear relationship between the global annual mean ITCZ response and the meridional SST gradient, regional and seasonal variations, particularly in the Pacific during DJF and the Atlantic during JJA, play a more significant role in shaping the relationship.

The geopotential height anomalies between LIGfw-lig127k and PIfw-piControl also display significant differences to the south of Australia, and so do the temperature anomalies in the Southern Ocean. The different temperature anomalies in the Southern Ocean are most likely due to the simulated warmer LIG Southern Ocean, with a 50% smaller sea-ice cover compared to PI in the ACCESS-ESM1.5 (Yeung et al., 2024). As such, future studies should more effectively assess how the coupled feedback, such as those between SST and wind changes in the high southern latitudes, could modulate regional precipitation anomalies in response to an AMOC weakening under varying background states.

4.2. Simulated Precipitation Comparison to Proxy Records and Future Implications

While we acknowledge the inconsistency among precipitation proxy records (as mentioned in Section 1), these discrepancies can be attributed to several factors, such as low temporal resolution, gaps in the records, and differences in the types of proxies used. Each proxy type may archive total precipitation differently, introducing uncertainties. Additionally, variations in past climate conditions, including differences in orbital parameters, vegetation cover, and regional climate dynamics, can also contribute to these inconsistencies. Despite these challenges, our simulated results are in agreement with those suggesting a decrease in precipitation over northern Borneo (Partin et al., 2007), and an increase over the Flores Sea (Ayliffe et al., 2013; Muller et al., 2012; Scroxton et al., 2022) and northern Australia (Denniston et al., 2013; Muller et al., 2008), during an AMOC shutdown. These similarities suggest that our model captures the broad regional trends, even though individual proxies may vary due to the reasons outlined above. Additionally, the precipitation anomalies are broadly similar to the precipitation minus evaporation anomalies (Figures S8 and S9 in Supporting Information S1), therefore consistent with proxy records of wetter conditions over northern Australia regardless of whether they reflect moisture balance or precipitation. Future work on high-resolution proxy records covering the LIG period would be invaluable in resolving some of these inconsistencies and enhancing model validation.

Due to the increase in greenhouse gas concentration, the global mean temperature was 1.4°C higher in 2023 than during PI, as confirmed by the World Meteorological Organization in their 2024 report. The warming trend, however, is much larger in the NH than in the SH, with the Arctic warming at four times the global rate (Rantanen et al., 2022), associated with a large sea-ice decrease (Jahn et al., 2024). As a result, the ITCZ has shifted northward at a rate of 30 km/decade over land (Aumann et al., 2024). CMIP6 Shared Socioeconomic Pathways (SSP5-8.5) simulations performed with the ACCESS-ESM1.5 (Mackallah et al., 2022) suggest that, despite a ~30% AMOC weakening (Weijer et al., 2020), the global annual mean position of the ITCZ could shift further northward at the end of the century (years 2080–2100) compared to PI (Figure 6a), driven by an enhanced meridional tropical SST gradient (5°N–30°N minus 5°N–30°S), with greater warming in the NH. This asymmetrical warming pattern, also observed during the LIG, makes the LIG a valuable analogue for understanding potential climate impacts of an AMOC weakening in the 21st-century, potentially amplified by Greenland ice-sheet and Arctic glacier melting (Pontes & Menviel, 2024).

5. Conclusions

Our study investigates the impact of an AMOC shutdown on precipitation patterns across the Australasian sector under two distinct climate background states: PI and LIG. While the overarching response to AMOC shutdown remains similar in both PI and LIG climates, our analysis unveils nuanced variations in Australasian hydroclimate patterns due to differences in the background state.

We highlight that the northern parts of Maritime continent and New Zealand experience drier conditions during both austral summer and winter, with subtle discrepancies under PI and LIG climate boundary conditions. However, during DJF, there is an increase in precipitation in northern Australia under both LIG and PI boundary conditions in response to the AMOC shutdown, but the increase is larger in LIG. During JJA, there is an increase in northwestern Australian precipitation coupled with a decrease in southeast Australia precipitation under LIG conditions, whereas under PI conditions, drier conditions are simulated all over Australia apart from the northern tip.

Considering the observed decrease in AMOC strength over the last 100 years and projected weakening in the future, our findings underscore the potential for substantial alterations in temperature gradients and atmospheric circulation, which could profoundly impact Australasian hydroclimate. By describing the simulated changes in both LIG and PI background states, our results offer valuable insights into the dynamic nature of climatic shifts and their implications for regional hydrological systems.

Data Availability Statement

The model outputs from all the simulations are available at (Saini et al., 2025).

Acknowledgments

Himadri Saini, Josephine R. Brown, Russell N. Drysdale, Yanxuan Du, and Laurie Menviel would like to acknowledge funding from the Australian Research Council (ARC) grant DP220102134. Gabriel Pontes and Laurie Menviel acknowledge support by ARC grant SR200100008. Model simulations were performed using the resources from the National Computational Infrastructure, which is supported by the Australian Government. Open access publishing facilitated by University of New South Wales, as part of the Wiley - University of New South Wales agreement via the Council of Australian University Librarians.

References

Aumann, H. H., Broberg, S., & Manning, E. M. (2024). Northward shift and narrowing of the ITCZ in 20 years of AIRS data. *Journal of Geophysical Research: Atmospheres*, *129*(5), e2023JD038723. https://doi.org/10.1029/2023jd038723

Ayliffe, L. K., Gagan, M. K., Zhao, J.-x., Drysdale, R. N., Hellstrom, J. C., Hantoro, W. S., et al. (2013). Rapid interhemispheric climate links via the Australasian monsoon during the last deglaciation. *Nature Communications*, *4*(1), 2908. https://doi.org/10.1038/ncomms3908

Beaufort, L., Van der Kaars, S., Bassinot, F., & Moron, V. (2010). Past dynamics of the Australian monsoon: Precession, phase and links to the global monsoon concept. *Climate of the Past*, *6*(5), 695–706. https://doi.org/10.5194/cp-6-695-2010

Berger, A. (1978). Long-term variations of daily insolation and quaternary climatic changes. *Journal of the Atmospheric Sciences*, *35*(12), 2362–2367. https://doi.org/10.1175/1520-0469(1978)035<2362:ltvodi>2.0.co;2

Blunier, T., & Brook, E. J. (2001). Timing of millennial-scale climate change in Antarctica and Greenland during the last glacial period. *Science*, *291*(5501), 109–112. https://doi.org/10.1126/science.291.5501.109

Boers, N. (2021). Observation-based early-warning signals for a collapse of the Atlantic meridional overturning circulation. *Nature Climate Change*, *11*(8), 680–688. https://doi.org/10.1038/s41558-021-01097-4

Braconnot, P., Otto-Bliesner, B., Harrison, S., Joussaume, S., Peterchmitt, J.-Y., Abe-Ouchi, A., et al. (2007). Results of PMIP2 coupled simulations of the mid-Holocene and Last Glacial Maximum–part 2: Feedbacks with emphasis on the location of the ITCZ and mid-and high latitudes heat budget. *Climate of the Past*, *3*(2), 279–296. https://doi.org/10.5194/cp-3-279-2007

Buizert, C., Cuffey, K., Severinghaus, J., Baggenstos, D., Fudge, T., Steig, E., et al. (2015). The WAIS Divide deep ice core WD2014 chronology–part 1: Methane synchronization (68–31 ka BP) and the gas age–ice age difference. *Climate of the Past*, *11*(2), 153–173. https://doi.org/10.5194/cp-11-153-2015

Buizert, C., Gkinis, V., Severinghaus, J. P., He, F., Lecavalier, B. S., Kindler, P., et al. (2014). Greenland temperature response to climate forcing during the last deglaciation. *Science*, *345*(6201), 1177–1180. https://doi.org/10.1126/science.1254961

Caesar, L., McCarthy, G. D., Thornalley, D., Cahill, N., & Rahmstorf, S. (2021). Current Atlantic meridional overturning circulation weakest in last millennium. *Nature Geoscience*, *14*(3), 118–120. https://doi.org/10.1038/s41561-021-00699-z

Caesar, L., Rahmstorf, S., Robinson, A., Feulner, G., & Saba, V. (2018). Observed fingerprint of a weakening Atlantic ocean overturning circulation. *Nature*, *556*(7700), 191–196. https://doi.org/10.1038/s41586-018-0006-5

Ciemer, C., Winkelmann, R., Kurths, J., & Boers, N. (2021). Impact of an AMOC weakening on the stability of the southern Amazon rainforest. *The European Physical Journal - Special Topics*, *230*(14), 3065–3073. https://doi.org/10.1140/epjs/s11734-021-00186-x

Clark, P. U., & Huybers, P. (2009). Interglacial and future sea level. *Nature*, *462*(7275), 856–857. https://doi.org/10.1038/462856a

Craig, A., Valcke, S., & Coquart, L. (2017). Development and performance of a new version of the OASIS coupler, OASIS3-MCT_3. 0. *Geoscientific Model Development*, *10*(9), 3297–3308. https://doi.org/10.5194/gmd-10-3297-2017

Cruz, F. W., Vuille, M., Burns, S. J., Wang, X., Cheng, H., Werner, M., et al. (2009). Orbitally driven east–west antiphasing of south American precipitation. *Nature Geoscience*, *2*(3), 210–214. https://doi.org/10.1038/ngeo444

Denniston, R. F., Wyrwoll, K.-H., Asmerom, Y., Polyak, V. J., Humphreys, W. F., Cugley, J., et al. (2013). North Atlantic forcing of millennial-scale Indo-Australian monsoon dynamics during the last glacial period. *Quaternary Science Reviews*, *72*, 159–168. https://doi.org/10.1016/j.quascirev.2013.04.012

Deplazes, G., Lückge, A., Peterson, L. C., Timmermann, A., Hamann, Y., Hughen, K. A., et al. (2013). Links between tropical rainfall and North Atlantic climate during the last glacial period. *Nature Geoscience*, *6*(3), 213–217. https://doi.org/10.1038/ngeo1712

Ditlevsen, P., & Ditlevsen, S. (2023). Warning of a forthcoming collapse of the Atlantic meridional overturning circulation. *Nature Communications*, *14*(1), 4254. https://doi.org/10.1038/s41467-023-39810-w

Dutton, A., & Lambeck, K. (2012). Ice volume and sea level during the Last Interglacial. *Science*, *337*(6091), 216–219. https://doi.org/10.1126/science.1205749

Dyer, B., Austermann, J., D'Andrea, W. J., Creel, R. C., Sandstrom, M. R., Cashman, M., et al. (2021). Sea-level trends across the Bahamas constrain peak Last Interglacial ice melt. *Proceedings of the National Academy of Sciences*, *118*(33), e2026839118. https://doi.org/10.1073/pnas.2026839118

Escobar, J., Hodell, D. A., Brenner, M., Curtis, J. H., Gilli, A., Mueller, A. D., et al. (2012). A 43-ka record of paleoenvironmental change in the central American lowlands inferred from stable isotopes of lacustrine ostracods. *Quaternary Science Reviews*, *37*, 92–104. https://doi.org/10.1016/j.quascirev.2012.01.020

Eyring, V., Bony, S., Meehl, G. A., Senior, C. A., Stevens, B., Stouffer, R. J., & Taylor, K. E. (2016). Overview of the Coupled Model Intercomparison Project phase 6 (CMIP6) experimental design and organization. *Geoscientific Model Development*, *9*(5), 1937–1958. https://doi.org/10.5194/gmd-9-1937-2016

Galaasen, E. V., Ninnemann, U. S., Irvalı, N., Kleiven, H. K. F., Rosenthal, Y., Kissel, C., & Hodell, D. A. (2014). Rapid reductions in North Atlantic deep water during the peak of the Last Interglacial period. *Science*, *343*(6175), 1129–1132. https://doi.org/10.1126/science.1248667

Galaasen, E. V., Ninnemann, U. S., Kessler, A., Irvalı, N., Rosenthal, Y., Tjiputra, J., et al. (2020). Interglacial instability of North Atlantic deep water ventilation. *Science*, *367*(6485), 1485–1489. https://doi.org/10.1126/science.aay6381

Gasse, F. (2000). Hydrological changes in the African tropics since the Last Glacial Maximum. *Quaternary Science Reviews*, *19*(1–5), 189–211. https://doi.org/10.1016/s0277-3791(99)00061-x

Griffies, S. M. (2012). Elements of the modular ocean model (mom). *GFDL Ocean Group Technical Report*, *7*(620), 47.

Haug, G. H., Hughen, K. A., Sigman, D. M., Peterson, L. C., & Rohl, U. (2001). Southward migration of the intertropical convergence zone through the Holocene. *Science*, *293*(5533), 1304–1308. https://doi.org/10.1126/science.1059725

Henry, L., McManus, J., Curry, W., Roberts, N., Piotrowski, A., & Keigwin, L. (2016). North Atlantic ocean circulation and abrupt climate change during the last glaciation. *Science*, *353*(6298), 470–474. https://doi.org/10.1126/science.aaf5529

Hoffman, J. S., Clark, P. U., Parnell, A. C., & He, F. (2017). Regional and global sea-surface temperatures during the Last Interglaciation. *Science*, *355*(6322), 276–279. https://doi.org/10.1126/science.aai8464

Huber, C., Leuenberger, M., Spahni, R., Flückiger, J., Schwander, J., Stocker, T. F., et al. (2006). Isotope calibrated Greenland temperature record over Marine Isotope Stage 3 and its relation to CH4. *Earth and Planetary Science Letters*, *243*(3–4), 504–519. https://doi.org/10.1016/j.epsl.2006.01.002

Hunke, E. C., Lipscomb, W. H., Turner, A. K., Jeffery, N., & Elliott, S. (2010). *CICE: The Los Alamos Sea Ice model documentation and software user's manual version 5.1 LA-CC-06-012. T-3 fluid dynamics group* (Vol. 675, p. 500). Los Alamos National Laboratory.
Jackson, L., Biastoch, A., Buckley, M. W., Desbruyères, D. G., Frajka-Williams, E., Moat, B., & Robson, J. (2022). The evolution of the North Atlantic meridional overturning circulation since 1980. *Nature Reviews Earth and Environment*, *3*(4), 241–254. https://doi.org/10.1038/s43017-022-00263-2
Jackson, L., Kahana, R., Graham, T., Ringer, M., Woollings, T., Mecking, J., & Wood, R. (2015). Global and European climate impacts of a slowdown of the AMOC in a high resolution GCM. *Climate Dynamics*, *45*(11–12), 3299–3316. https://doi.org/10.1007/s00382-015-2540-2
Jahn, A., Holland, M. M., & Kay, J. E. (2024). Projections of an ice-free Arctic ocean. *Nature Reviews Earth and Environment*, *5*(3), 1–13. https://doi.org/10.1038/s43017-023-00515-9
Jennerjahn, T. C., Ittekkot, V., Arz, H. W., Behling, H., Patzold, J., & Wefer, G. (2004). Asynchronous terrestrial and marine signals of climate change during Heinrich events. *Science*, *306*(5705), 2236–2239. https://doi.org/10.1126/science.1102490
Jouzel, J., Masson-Delmotte, V., Cattani, O., Dreyfus, G., Falourd, S., Hoffmann, G., et al. (2007). Orbital and millennial Antarctic climate variability over the past 800,000 years. *Science*, *317*(5839), 793–796. https://doi.org/10.1126/science.1141038
Kageyama, M., Merkel, U., Otto-Bliesner, B., Prange, M., Abe-Ouchi, A., Lohmann, G., et al. (2013). Climatic impacts of fresh water hosing under Last Glacial Maximum conditions: A multi-model study. *Climate of the Past*, *9*(2), 935–953. https://doi.org/10.5194/cp-9-935-2013
Kageyama, M., Sime, L. C., Sicard, M., Guarino, M.-V., de Vernal, A., Schroeder, D., et al. (2020). A multi-model CMIP6 study of Arctic sea ice at 127 ka: Sea ice data compilation and model differences. *Climate of the Past Discussions*, *2020*, 1–33.
Kindler, P., Guillevic, M., Baumgartner, M. F., Schwander, J., Landais, A., & Leuenberger, M. (2014). Temperature reconstruction from 10 to 120 kyr b2k from the NGRIP ice core. *Climate of the Past*, *10*(2), 887–902. https://doi.org/10.5194/cp-10-887-2014
Kopp, R. E., Simons, F. J., Mitrovica, J. X., Maloof, A. C., & Oppenheimer, M. (2009). Probabilistic assessment of sea level during the Last Interglacial stage. *Nature*, *462*(7275), 863–867. https://doi.org/10.1038/nature08686
Kowalczyk, E., Stevens, L., Law, R., Dix, M., Wang, Y., Harman, I., et al. (2013). The land surface model component of access: Description and impact on the simulated surface climatology. *Australian Meteorological and Oceanographic Journal*, *63*(1), 65–82. https://doi.org/10.22499/2.6301.005
Laskar, J., Robutel, P., Joutel, F., Gastineau, M., Correia, A. C., & Levrard, B. (2004). A long-term numerical solution for the insolation quantities of the earth. *Astronomy and Astrophysics*, *428*(1), 261–285. https://doi.org/10.1051/0004-6361:20041335
Latif, M., Sun, J., Visbeck, M., & Hadi Bordbar, M. (2022). Natural variability has dominated Atlantic meridional overturning circulation since 1900. *Nature Climate Change*, *12*(5), 455–460. https://doi.org/10.1038/s41558-022-01342-4
Lewis, S. C., Gagan, M. K., Ayliffe, L. K., Zhao, J.-x., Hantoro, W. S., Treble, P. C., et al. (2011). High-resolution stalagmite reconstructions of Australian–Indonesian monsoon rainfall variability during Heinrich stadial 3 and Greenland Interstadial 4. *Earth and Planetary Science Letters*, *303*(1–2), 133–142. https://doi.org/10.1016/j.epsl.2010.12.048
Lynch-Stieglitz, J. (2017). The Atlantic meridional overturning circulation and abrupt climate change. *Annual Review of Marine Science*, *9*(1), 83–104. https://doi.org/10.1146/annurev-marine-010816-060415
Mackallah, C., Chamberlain, M., Law, R., Dix, M., Ziehn, T., Bi, D., et al. (2022). Access datasets for CMIP6: Methodology and idealised experiments. *Journal of Southern Hemisphere Earth Systems Science*, *72*(2), 93–116. https://doi.org/10.1071/es21031
Martin, G., Milton, S., Senior, C., Brooks, M., Ineson, S., Reichler, T., & Kim, J. (2010). Analysis and reduction of systematic errors through a seamless approach to modeling weather and climate. *Journal of Climate*, *23*(22), 5933–5957. https://doi.org/10.1175/2010jcli3541.1
The HadGEM2 Development Team: Martin, G. M., Bellouin, N., Bellouin, N., Collins, W., Culverwell, I., Halloran, P., et al. (2011). The HADGEM2 family of met office unified model climate configurations. *Geoscientific Model Development*, *4*(3), 723–757. https://doi.org/10.5194/gmd-4-723-2011
Masson-Delmotte, V., Schulz, M., Abe-Ouchi, A., Beer, J., Ganopolski, A., Rouco, J. G., et al. (2013). Information from paleoclimate archives. In *Climate change 2013: The physical science basis contribution of working group i to the fifth assessment report of the intergovernmental panel on climate change*.
McGee, D., de Menocal, P. B., Winckler, G., Stuut, J.-B. W., & Bradtmiller, L. (2013). The magnitude, timing and abruptness of changes in North African dust deposition over the last 20,000 yr. *Earth and Planetary Science Letters*, *371*, 163–176. https://doi.org/10.1016/j.epsl.2013.03.054
McGee, D., Donohoe, A., Marshall, J., & Ferreira, D. (2014). Changes in ITCZ location and cross-equatorial heat transport at the Last Glacial Maximum, Heinrich stadial 1, and the mid-Holocene. *Earth and Planetary Science Letters*, *390*, 69–79. https://doi.org/10.1016/j.epsl.2013.12.043
Menviel, L., Capron, E., Govin, A., Dutton, A., Tarasov, L., Abe-Ouchi, A., et al. (2019). The penultimate deglaciation: Protocol for Paleoclimate Modelling Intercomparison Project (PMIP) phase 4 transient numerical simulations between 140 and 127 ka, version 1.0. *Geoscientific Model Development*, *12*(8), 3649–3685. https://doi.org/10.5194/gmd-12-3649-2019
Menviel, L., England, M. H., Meissner, K. J., Mouchet, A., & Yu, J. (2014). Atlantic-Pacific seesaw and its role in outgassing CO_2 during Heinrich events. *Paleoceanography*, *29*(1), 58–70. https://doi.org/10.1002/2013pa002542
Menviel, L., Skinner, L. C., Tarasov, L., & Tzedakis, P. C. (2020). An ice–climate oscillatory framework for Dansgaard–Oeschger cycles. *Nature Reviews Earth and Environment*, *1*(12), 677–693. https://doi.org/10.1038/s43017-020-00106-y
Menviel, L., Timmermann, A., Friedrich, T., & England, M. H. (2014). Hindcasting the continuum of Dansgaard–Oeschger variability: Mechanisms, patterns and timing. *Climate of the Past*, *10*(1), 63–77. https://doi.org/10.5194/cp-10-63-2014
Menviel, L., Timmermann, A., Mouchet, A., & Timm, O. (2008). Meridional reorganizations of marine and terrestrial productivity during Heinrich events. *Paleoceanography*, *23*(1). https://doi.org/10.1029/2007pa001445
Mohtadi, M., Oppo, D. W., Steinke, S., Stuut, J.-B. W., De Pol-Holz, R., Hebbeln, D., & Lückge, A. (2011). Glacial to Holocene swings of the Australian–Indonesian monsoon. *Nature Geoscience*, *4*(8), 540–544. https://doi.org/10.1038/ngeo1209
Muller, J., Kylander, M., Wüst, R. A., Weiss, D., Martinez-Cortizas, A., LeGrande, A. N., et al. (2008). Possible evidence for wet Heinrich phases in tropical NE Australia: The Lynch's Crater deposit. *Quaternary Science Reviews*, *27*(5–6), 468–475. https://doi.org/10.1016/j.quascirev.2007.11.006
Muller, J., McManus, J. F., Oppo, D. W., & Francois, R. (2012). Strengthening of the northeast monsoon over the flores sea, Indonesia, at the time of heinrich event 1. *Geology*, *40*(7), 635–638. https://doi.org/10.1130/g32878.1
Muschitiello, F., D'Andrea, W. J., Schmittner, A., Heaton, T. J., Balascio, N. L., DeRoberts, N., et al. (2019). Deep-water circulation changes lead North Atlantic climate during deglaciation. *Nature Communications*, *10*(1), 1272. https://doi.org/10.1038/s41467-019-09237-3
Oke, P. R., Griffin, D. A., Schiller, A., Matear, R., Fiedler, R., Mansbridge, J., et al. (2013). Evaluation of a near-global eddy-resolving ocean model. *Geoscientific Model Development*, *6*(3), 591–615. https://doi.org/10.5194/gmd-6-591-2013
Okumura, Y. M., Deser, C., Hu, A., Timmermann, A., & Xie, S.-P. (2009). North pacific climate response to freshwater forcing in the subarctic north atlantic: Oceanic and atmospheric pathways. *Journal of Climate*, *22*(6), 1424–1445. https://doi.org/10.1175/2008jcli2511.1

Orihuela-Pinto, B., England, M. H., & Taschetto, A. S. (2022). Interbasin and interhemispheric impacts of a collapsed atlantic overturning circulation. *Nature Climate Change*, *12*(6), 558–565. https://doi.org/10.1038/s41558-022-01380-y

Otto-Bliesner, B. L., Braconnot, P., Harrison, S. P., Lunt, D. J., Abe-Ouchi, A., Albani, S., et al. (2017). The PMIP4 contribution to CMIP6–part 2: Two interglacials, scientific objective and experimental design for holocene and last interglacial simulations. *Geoscientific Model Development*, *10*(11), 3979–4003. https://doi.org/10.5194/gmd-10-3979-2017

Otto-Bliesner, B. L., Brady, E. C., Zhao, A., Brierley, C. M., Axford, Y. L., Capron, E., et al. (2021). Large-scale features of Last Interglacial climate: Results from evaluating the lig127k simulations for the coupled model intercomparison project (CMIP6)-paleoclimate modeling intercomparison project (PMIP4). *Climate of the Past*, *17*(1), 63–94. https://doi.org/10.5194/cp-17-63-2021

Partin, J. W., Cobb, K. M., Adkins, J. F., Clark, B., & Fernandez, D. P. (2007). Millennial-scale trends in west pacific warm pool hydrology since the Last Glacial Maximum. *Nature*, *449*(7161), 452–455. https://doi.org/10.1038/nature06164

Pedro, J. B., Jochum, M., Buizert, C., He, F., Barker, S., & Rasmussen, S. O. (2018). Beyond the bipolar seesaw: Toward a process understanding of interhemispheric coupling. *Quaternary Science Reviews*, *192*, 27–46. https://doi.org/10.1016/j.quascirev.2018.05.005

Peterson, L. C., Haug, G. H., Hughen, K. A., & Rohl, U. (2000). Rapid changes in the hydrologic cycle of the tropical atlantic during the last glacial. *Science*, *290*(5498), 1947–1951. https://doi.org/10.1126/science.290.5498.1947

Pontes, G. M., & Menviel, L. (2024). Weakening of the Atlantic meridional overturning circulation driven by subarctic freshening since the mid-twentieth century. *Nature Geoscience*, *17*(12), 1291–1298. https://doi.org/10.1038/s41561-024-01568-1

Rahmstorf, S. (2002). Ocean circulation and climate during the past 120,000 years. *Nature*, *419*(6903), 207–214. https://doi.org/10.1038/nature01090

Rahmstorf, S., Box, J. E., Feulner, G., Mann, M. E., Robinson, A., Rutherford, S., & Schaffernicht, E. J. (2015). Exceptional twentieth-century slowdown in Atlantic ocean overturning circulation. *Nature Climate Change*, *5*(5), 475–480. https://doi.org/10.1038/nclimate2554

Rantanen, M., Karpechko, A. Y., Lipponen, A., Nordling, K., Hyvärinen, O., Ruosteenoja, K., et al. (2022). The Arctic has warmed nearly four times faster than the globe since 1979. *Communications Earth and Environment*, *3*(1), 168. https://doi.org/10.1038/s43247-022-00498-3

Saini, H., Meissner, K. J., Menviel, L., & Kvale, K. (2024). Transient response of Southern Ocean ecosystems during Heinrich stadials. *Paleoceanography and Paleoclimatology*, *39*(2), e2023PA004754. https://doi.org/10.1029/2023pa004754

Saini, H., Pontes, G. M., Brown, J. R., Drysdale, R., Du, Y., & Menviel, L. (2025). Access model outputs for FW simulations under PI and LIG boundary conditions. *Dryad*. [Dataset]. https://doi.org/10.5061/dryad.5qfttdzfw

Schneider, T., Bischoff, T., & Haug, G. H. (2014). Migrations and dynamics of the intertropical convergence zone. *Nature*, *513*(7516), 45–53. https://doi.org/10.1038/nature13636

Scroxton, N., Gagan, M. K., Ayliffe, L. K., Hantoro, W. S., Hellstrom, J. C., Cheng, H., et al. (2022). Antiphase response of the Indonesian–Australian monsoon to millennial-scale events of the last glacial period. *Scientific Reports*, *12*(1), 20214. https://doi.org/10.1038/s41598-022-21843-8

Seidov, D., & Maslin, M. (2001). Atlantic ocean heat piracy and the bipolar climate see-saw during Heinrich and Dansgaard–Oeschger events. *Journal of Quaternary Science: Published for the Quaternary Research Association*, *16*(4), 321–328. https://doi.org/10.1002/jqs.595

Smeed, D. A., Josey, S., Beaulieu, C., Johns, W., Moat, B. I., Frajka-Williams, E., et al. (2018). The North Atlantic Ocean is in a state of reduced overturning. *Geophysical Research Letters*, *45*(3), 1527–1533. https://doi.org/10.1002/2017gl076350

Stocker, T. F. (1998). The seesaw effect. *Science*, *282*(5386), 61–62. https://doi.org/10.1126/science.282.5386.61

Stocker, T. F., & Johnsen, S. J. (2003). A minimum thermodynamic model for the bipolar seesaw. *Paleoceanography*, *18*(4). https://doi.org/10.1029/2003pa000920

Stouffer, R. J., Yin, J.-j., Gregory, J., Dixon, K., Spelman, M., Hurlin, W., et al. (2006). Investigating the causes of the response of the thermohaline circulation to past and future climate changes. *Journal of Climate*, *19*(8), 1365–1387. https://doi.org/10.1175/jcli3689.1

Thornalley, D. J., Oppo, D. W., Ortega, P., Robson, J. I., Brierley, C. M., Davis, R., et al. (2018). Anomalously weak labrador sea convection and atlantic overturning during the past 150 years. *Nature*, *556*(7700), 227–230. https://doi.org/10.1038/s41586-018-0007-4

Timmermann, A., Menviel, L., Okumura, Y., Schilla, A., Merkel, U., Timm, O., et al. (2010). Towards a quantitative understanding of millennial-scale antarctic warming events. *Quaternary Science Reviews*, *29*(1–2), 74–85. https://doi.org/10.1016/j.quascirev.2009.06.021

Tzedakis, P. C., Drysdale, R. N., Margari, V., Skinner, L. C., Menviel, L., Rhodes, R. H., et al. (2018). Enhanced climate instability in the north atlantic and southern europe during the last interglacial. *Nature Communications*, *9*(1), 4235. https://doi.org/10.1038/s41467-018-06683-3

Vellinga, M., & Wood, R. A. (2002). Global climatic impacts of a collapse of the Atlantic thermohaline circulation. *Climatic Change*, *54*(3), 251–267. https://doi.org/10.1023/a:1016168827653

Wang, B., Kim, H.-J., Kikuchi, K., & Kitoh, A. (2011). Diagnostic metrics for evaluation of annual and diurnal cycles. *Climate Dynamics*, *37*(5–6), 941–955. https://doi.org/10.1007/s00382-010-0877-0

Wang, X., Auler, A. S., Edwards, R. L., Cheng, H., Cristalli, P. S., Smart, P. L., et al. (2004). Wet periods in northeastern Brazil over the past 210 kyr linked to distant climate anomalies. *Nature*, *432*(7018), 740–743. https://doi.org/10.1038/nature03067

Wang, Y., Law, R., & Pak, B. (2010). A global model of carbon, nitrogen and phosphorus cycles for the terrestrial biosphere. *Biogeosciences*, *7*(7), 2261–2282. https://doi.org/10.5194/bg-7-2261-2010

Weijer, W., Cheng, W., Garuba, O. A., Hu, A., & Nadiga, B. (2020). CMIP6 models predict significant 21st century decline of the Atlantic meridional overturning circulation. *Geophysical Research Letters*, *47*(12), e2019GL086075. https://doi.org/10.1029/2019gl086075

Weldeab, S., Lea, D. W., Schneider, R. R., & Andersen, N. (2007). 155,000 years of west african monsoon and ocean thermal evolution. *Science*, *316*(5829), 1303–1307. https://doi.org/10.1126/science.1140461

Wyrwoll, K.-H., Liu, Z., Chen, G., Kutzbach, J. E., & Liu, X. (2007). Sensitivity of the Australian summer monsoon to tilt and precession forcing. *Quaternary Science Reviews*, *26*(25–28), 3043–3057. https://doi.org/10.1016/j.quascirev.2007.06.026

Yeung, N. K.-H., Menviel, L., Meissner, K. J., Choudhury, D., Ziehn, T., & Chamberlain, M. A. (2024). Last interglacial subsurface warming on the antarctic shelf triggered by reduced deep-ocean convection. *Communications Earth and Environment*, *5*(1), 212. https://doi.org/10.1038/s43247-024-01383-x

Yeung, N. K.-H., Menviel, L., Meissner, K. J., Taschetto, A. S., Ziehn, T., & Chamberlain, M. (2021). Land–sea temperature contrasts at the last interglacial and their impact on the hydrological cycle. *Climate of the Past*, *17*(2), 869–885. https://doi.org/10.5194/cp-17-869-2021

Zhang, P., Xu, J., Holbourn, A., Kuhnt, W., Xiong, Z., & Li, T. (2022). Obliquity induced latitudinal migration of the intertropical convergence zone during the past 410 kyr. *Geophysical Research Letters*, *49*(21), e2022GL100039. https://doi.org/10.1029/2022gl100039

Ziehn, T., Chamberlain, M. A., Law, R. M., Lenton, A., Bodman, R. W., Dix, M., et al. (2020). The australian earth system model: Access-esm1. 5. *Journal of Southern Hemisphere Earth Systems Science*, *70*(1), 193–214. https://doi.org/10.1071/es19035